Water Chain Formation and Possible Proton Pumping Routes in *Rhodobacter sphaeroides* Cytochrome *c* Oxidase: A Molecular Dynamics Comparison of the Wild Type and R481K Mutant†

Steve A. Seibold,‡,§ Denise A. Mills,|| Shelagh Ferguson-Miller,|| and Robert I. Cukier*,‡,§

Department of Chemistry, Department of Biochemistry and Molecular Biology, and Center for Biological Modeling, Michigan State University, East Lansing, Michigan 48824

Received February 17, 2005; Revised Manuscript Received May 23, 2005

ABSTRACT: Cytochrome *c* oxidase (C*c*O) converts the energy from redox and oxygen chemistry to support proton translocation and create a transmembrane $\Delta\mu H^+$ used for ATP production. Molecular dynamics (MD) simulations were carried out to probe for the formation water chains capable of participating in proton translocation. Attention was focused on the region between and above the *a* and a_3 hemes where well-defined water chains have not been identified in crystallographic studies. An arginine (R481) (*Rhodobacter sphaeroides* numbering), positioned between the D-propionates of the hemes, had been mutated in vivo to lysine and showed to have altered activity consistent with an altered proton conductance [Qian, J., Mills, D. A., Geren, L., Wang, K. F., Hoganson, C. W., Schmidt, B., Hiser, C., Babcock, G. T., Durham, B., Millett, F., and Ferguson-Miller, S. (2004) Role of the conserved arginine pair in proton and electron transfer in cytochrome *c* oxidase, *Biochemistry 43,* 5748−5756; also see the accompanying paper by Mills et al.]. This mutant was created in silico, and the MD results for the mutant and wild type were compared to explore the effects on the formation of hydrogen-bonded water chains by this mutation. The simulations reveal the presence of hydrogen-bonded water chains that lead from E286 through the region above the hemes to the Mg^{2+}, and from E286 to the heme a_3 D-propionate and the binuclear center. The R481K mutant does not form as many, or as extensive, water chains as wild-type C*c*O, due to a new conformation of residues in a large loop between helices III and IV in subunit I, indicating a reduction in the level of water chain formation in the mutant. This loop appears to play a role in controlling the formation of hydrogen-bonded water chains above the hemes. The results suggest a possible gating mechanism for proton movement that includes key residues W172 and Y175 on the loop and F282 on helix VI.

The terminal electron transfer protein in most aerobic organisms is the multisubunit enzyme complex cytochrome *c* oxidase (C*c*O)[1] (*2*). It reduces oxygen to water and pumps protons from one side of the membrane (interior "in") to the other (exterior "out") according to the stoichiometry

$$4e^- + 8H_{in}{}^+ + O_2 \rightarrow 4H_{out}{}^+ + 2H_2O$$

that leads to the establishment of an $\Delta\mu H^+$ across the membrane and provides the energy for ATP synthesis. Despite the intensive study of C*c*O, the mechanism of proton translocation through the protein, its coupling to electron transfer reactions, and to oxygen reduction is not well understood (*3*−*6*). Mitchell and Rich (*7*) postulated that electroneutrality is used to drive protonation changes in the interior of the protein and at the binuclear center. This has led to models in which each electron transferred to heme *a* is accompanied by an uptake or movement of one proton to the interior (*8*−*10*). The electron on heme *a* is then transferred to the heme a_3 site. With this reduction of heme a_3, another proton to be used in oxygen reduction is brought to the catalytic binuclear site and the previously loaded proton in the vicinity of the heme *a* site is released toward the exterior (pumped). In this model, these events are driven by the necessity of preserving the electroneutrality of the system in the protein interior. Whatever the mechanism in moving protons in C*c*O, it must account for the unidirectional proton translocation event, which occurs against an $\Delta\mu H^+$, an endergonic process.

It has been convincingly demonstrated that certain amino acids are involved in movement of protons into the interior of the protein. These residues define the location of two proton uptake pathways called the D and K pathway for key residues D132 and K362 [numbering is for *Rhodobacter*

† The financial support of the National Institutes of Health (Grant GM47274 to R.I.C. and Grant GM26916 to S.F.-M.) is gratefully acknowledged.

* To whom correspondence should be addressed: Department of Chemistry, Michigan State University, East Lansing, MI 48824. Fax: (517) 353-1793. Telephone: (517) 355-9715, ext. 263. E-mail: cukier@cem.msu.edu.

‡ Department of Chemistry.

§ Center for Biological Modeling.

|| Department of Biochemistry and Molecular Biology.

[1] Abbreviations: C*c*O, cytochrome *c* oxidase; FTIR, Fourier transform infrared spectroscopy; MD, molecular dynamics; *Rs*, *Rhodobacter sphaeroides*; TW, test water; WT, wild-type; $\Delta\mu H^+$, electrochemical gradient potential of H^+.

10.1021/bi0502902 CCC: $30.25
Published on Web 07/14/2005

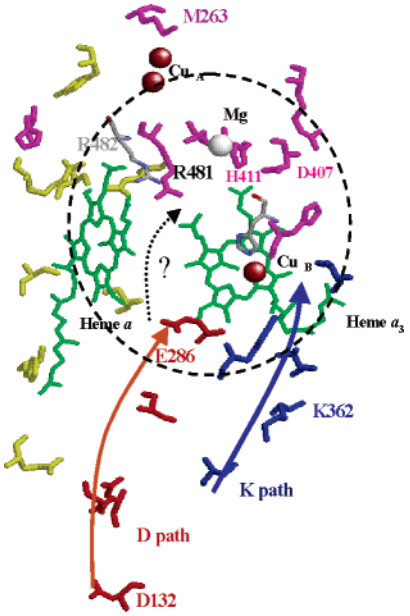

FIGURE 1: Two pathways (D and K path, solid arrows) in *Rs* cytochrome *c* oxidase that have been proposed to support chains of hydrogen-bonded waters that could transport protons into the periphery of the catalytic center (dashed circle). The defined D path ends at E286 but is thought to extend (dotted arrow) into the catalytic center, although no direct path has been verified.

sphaeroides (*Rs*) C*c*O], respectively (Figure 1). The D path is thought to be the major pathway for both pumped and substrate protons (*11*, *12*). Biochemical studies and observation of crystallographic waters have lead to the proposition that the protons move up the D pathway to the critical residue, E286 (*13*, *14*). However, the pathway for protons beyond E286 is not apparent from structural or functional studies. Some, however, have speculated that protons are passed to the heme propionates (both *a* and a_3) and to the binuclear center through a water-mediated mechanism that may involve specific amino acids, and/or water chains (see Figure 1) (*15*, *16*). The identification of the proton-accepting groups and those guiding the movement of water in these pathways are essential for understanding the mechanism of proton movement for both pumping and oxygen chemistry.

Proton translocation through C*c*O is thought to be facilitated, in part, by the formation of hydrogen-bonded water chains. These hydrogen-bonded waters might transport protons using the Grotthuss mechanism (*17*, *18*). The structural data on *Rs* C*c*O reveal a D pathway starting on D132 (cf. Figure 1), which could transport protons to E286 (*14*, *19*). Simulated annealing and free energy molecular dynamic studies suggested that conformational changes of E286 could assist in proton translocation and are kinetically feasible (*20*). Recent simulations, using constraints and a limited number of waters, have been performed on wild-type C*c*O (*21*−*23*). Wikstrom et al. (*22*) investigated the formation of water chains in wild-type *Rs* C*c*O by examining a 30 Å radius sphere around the hemes with all atoms constrained, except for a few residues around the active center. They found that arbitrarily placing three to five water molecules in a cavity near the oxidized binuclear center (Cu_B^{2+} and Fe^{3+}), with heme *a* reduced, followed by a 200 ps simulation resulted in the formation of a water chain consisting of two waters extending from E286 to W172 or to the oxidized heme a_3 D-propionate. In contrast, when heme *a* was oxidized and the binuclear center was reduced, they found three waters connecting E286 to the hydroxyl group on Cu_B. In a study by Zheng et al. (*24*), nine water molecules were manually placed in the heme a_3 catalytic pocket sequentially, running short dynamic steps before the addition of each water molecule. These MD simulations were carried out with most of the protein constrained. They were able to generate a water chain that started at the heme a_3 iron and extended to its D-propionate. E286 was also within hydrogen bonding distance of this water chain. Cukier (*3*) investigated water chain formation by MD in well-solvated, fully reduced wild-type *Rs* C*c*O, without any enzyme or water constraints. Waters were initially placed in the enzyme by an algorithm designed to find possible stable water locations. The simulations revealed that numerous transient water chains could form in various regions of the protein, including robust chains spanning E286 and Mg^{2+}. These water chains are limited in lifetime, but constantly form and re-form and on average are quite persistent. A typical snapshot showed a continuous hydrogen-bonded 13-water chain spanning E286 to Mg^{2+} that passes over the heme a_3 binuclear center.

The involvement of specific residue R481 is suggested by its position in the crystal structure where NH1 and NH2 are within hydrogen bonding distance (3.2 and 3.4 Å, respectively) of the heme a_3 D-propionate (*14*). The C*c*O mutants, R481N and R481L, in *Escherichia coli* both exhibit a loss of proton pumping, again suggesting the involvement of R481 in proton translocation (*16*). FTIR has implicated conformational and/or protonation changes for two heme propionate side chains upon reduction of the enzyme (*25*). Using mutants of C*c*O, Behr et al., in an FTIR study, later concluded that the D-propionate of heme *a* was the most likely candidate for proton acceptance, although the heme a_3 D-propionate might also undergo conformational changes and/or act as a proton donor (*26*). Although crystal structures have not revealed hydrogen-bonded water chains in this region, water molecules are consistently found at specific sites, including some around the heme *a* and heme a_3 propionates, again illustrating their possible involvement in proton pumping (*14*, *27*, *28*).

An R481 mutant of particular interest is R481K because this conservative mutation retains the positive charge and is unlikely to cause structural rearrangement, but is likely to interact differently with the heme propionates than the highly conserved arginine. Recent biochemical studies on this mutation show that C*c*O is still capable of reducing oxygen and pumping protons but that this activity is slower than that of the wild type (*1*). These studies (*15*, *16*) point to a role of R481 in proton pumping and activity. In addition, the activity of the R481K mutant is markedly inhibited in the presence of a membrane potential (*1*). Therefore, in this work, we perform a MD study of the mutant R481K to help define the role of R481 in enzyme activity, and to understand how the R481K mutant might disrupt its activity. The simulations were performed in the presence of explicit waters without any restraints on the protein or water. A comparison of the results of this simulation with those of the previous wild-type simulation (*3*) should help to determine how the arginine might influence proton movement above the hemes. To this end, the formation and persistence of water chains extending from E286 to the terminal sites, including Mg^{2+},

heme a_3 D-propionate, and the Cu_B and heme a_3 Fe, are investigated for the R481K mutant, and the results are compared with those of wild-type *Rs* C*c*O. The mutant is found to be deficient relative to the wild type in its ability to form hydrogen-bonded water chains in the regions between E286 and the binuclear site and between E286 and the Mg^{2+}. We trace this distinction in the mutant to a major structural change in a loop (carrying conserved residues W172 and Y175) connecting helices III and IV. The structural change results in the collapse of what, in the wild type, appears to be a hydrophobic tunnel that allows access of waters from E286 to the three terminal sites listed above.

COMPUTATIONAL METHODOLOGY

Molecular Dynamics. The molecular dynamics simulation were carried out using CUKMODY, a code designed for the efficient simulation of proteins and other large solutes (*29*). The GROMOS force field (*30*) for the residues and water is used in CUKMODY. The additions to the force field required to simulate C*c*O are discussed below. A combination of a cell index method with linked lists (*31*) and a Verlet neighbor list (*32*) is used to provide linear scaling with the number of atoms in the pair list routine. The electrostatic interactions are evaluated using the charge group method, to be consistent with the parametrization of the GROMOS force field. Periodic boundary conditions are used. The SHAKE algorithm (*33*) is used to constrain bond lengths permitting a 2 fs time step. The simulation is carried out at constant NVT with velocity scaling to control the temperature to around 300 K (*34*). The startup protocol creates a face-centered cubic lattice of water molecules, and centers the protein in the simulation cell, and waters that overlap the protein are discarded. The simulation is started with the protein cold, and the solvent heats the protein as the solvent molecules equilibrate to each other and the protein.

The initial configuration for the wild-type molecular dynamics is a preliminary version (*35*) of the recently published X-ray crystal structure of *Rs* C*c*O (*14*). The mutant was constructed by replacing Arg481 with Lys in the crystal structure, and then energy minimizing the lysine side chain interactions by use of the MOE-Rotamer Explorer and the CHARMm force field (*36*, *37*). The simulated system consisted of subunits I and II, with polar hydrogens added by use of the MOE program, and the 18 399 water molecules left in the simulation box after elimination of the waters that overlapped the protein. The box side is 88.7 Å long, and the largest dimension of C*c*O is ~80 Å, leaving ~20 Å between protein molecules in neighboring cells. The large number of waters facilitates investigation of the formation of hydrogen-bonded water structures.

The histidine residues are assumed to be neutral (singly protonated); the aspartic and glutamic acids are ionized (−1), and the lysines and arginines are protonated (+1). While the pK_a of E286 is known to be unusually high, the simulation is carried out for it being deprotonated. To conduct protons, E286 must be deprotonated part of the time, and because the wild-type simulations were carried out for the deprotonated state, we maintained this charge state for purposes of comparison. A force field for the two heme *a*'s (with their farnesyl "tails") was constructed starting from the GROMOS force field's heme *c*. The porphyrin charge distribution was maintained and the farnesyl chain modeled with charges appropriate for a hydrocarbon chain with the added hydroxyl group. The propionate groups are assumed to be ionized. Both heme groups are assumed to be in their reduced states, with a formal charge of Fe^{2+}. Cu_B, also assumed to be reduced (+1), is ligated to three histidine residues (H284, H333, and H334). With charge delocalization to these histidines, the MD charge of Cu_B is assigned as +0.41, a value essentially the same as that used in Hofacker and Schulten's C*c*O study (*38*). The Y288 ring C6 and H284 NE (ϵ-nitrogen on the imidazole ring) atoms are covalently linked, in accord with crystallographic results (*14*). The Cu_A-Cu_A site forms a I−II mixed valence compound (Robin-Day type III) leading to formal charges of +1.5 per Cu_A (*39*). One Cu_A is ligated to E54, C256, and H260 and the other to H217, C252, and M263. For MD purposes, the charges are assigned as +0.75 per Cu_A, because of the charge transfer to the (deprotonated) cysteine ligands. The two His ligands are assigned a charge of +0.25, and each of the two (deprotonated) cysteine ligands is assigned a total charge of −0.5 (*38*). The magnesium and calcium ions are assigned their formal charges of +2.

Water Insertion. The elimination of waters, defined on a lattice, that overlap protein atoms may still leave space for additional waters within the protein. A search for places for additional interior waters was carried out by first scanning a van der Waals test sphere, with water's van der Waals diameter, over a grid with spacing of 1.5 Å in each of the three Cartesian coordinate directions and recording candidate test spheres if their total interaction energy with neighboring atoms was less than 2 kcal/mol. Each candidate is made into a potential test water (TW) by inserting water's electrostatic charges, spinning it over a set of 18 orientations, evaluating the energy for each orientation, and recording the minimum-energy one. Carrying out this procedure for all candidates and accepting all whose energy lies below −2 kcal/mol provides a refined set of TWs. (Different choices for the energetic cutoffs lead to similar results, as long as the van der Waals energy is not made to be very large or the electrostatic energy very negative.) Some of these waters were close to each other, because of the 1.5 Å grid spacing that we used. For those that are within hydrogen bonding distance (oxygen−oxygen distance of <2.7 Å), one of the pair was eliminated. This algorithm was used to insert approximately 500 more waters into the protein, and they are included in the molecular dynamics simulation. The numbers of TWs in the wild-type and mutant forms are equal.

Channel Definition and Water Chain Algorithm. The channel definition adopted here constructs a cylinder, typically with a radius of 10 Å, whose axis begins on one atom and terminates on another. All waters within a cylinder are written to a file every 0.1 ps for further analysis. With this frequent interrogation of water configurations, we can assess the statistics of chain formation and destruction and catch "rare" configurations. It should be appreciated that within the intrinsically short MD simulation time scale of nanosecond, especially for a large protein with a large number of solvating waters that requires a great deal of processing time for the simulation, rare configurations are not easy to capture.

A program we developed to construct hydrogen-bonded water "trees" was then used to identify interesting water−

protein structures in each cylinder (*29*). A tree is constructed by first selecting a "root" water, typically at one end of the cylinder, which is hydrogen bonded to a residue, metal, or cofactor. All waters (level 1) that are hydrogen bonded to the root (level 0) are stored, and the root is removed from the list of possible hydrogen bond formers. Each level 1 water is, in turn, considered as a root; all waters hydrogen bonded to each of these are stored (level 2) and all level 1 waters removed from the list of possible hydrogen bond formers, and this procedure is continued recursively. Picking a desired number of levels, N_{lev}, will then produce, for all the MD steps considered, all trees of hydrogen-bonded waters with a length of at least N_{lev}. A terminal water can also be specified, often selected at the end of the channel and itself hydrogen bonded to a residue, metal, or cofactor, leading to the identification of water trees with given origin and termination points. The criterion for hydrogen bond formation can be varied from, for example, "easy" where all members of a tree have an Oa−Ob distance (d_{Oa-Ob}) between the oxygens of waters a and b of <3.5 Å to "severe" where d_{Oa-Ob} < 3.0 Å and the Oa−H−Ob angle $A_{Oa-H-Ob}$ is between 145° and 180°.

Persistent Waters Algorithm. Most of the waters that are displayed in the figures are eventually replaced with other waters, though some (that we shall note at the appropriate places) are quite persistent. Clearly, the persistence time requires an operational definition both for duration and for how far the water can move and still be hydrogen bonded to a particular residue. For a given hydrogen-bonded structure, where there is a water chain connecting two residues, at some other nearby instant of time the chain may be broken in one or more places, and shortly thereafter, it may re-form. Thus, while we provide snapshots of chains, it should be evident that they are forming and re-forming dynamically. Of course, for a given data set, the percentage of complete chains will also depend on the definition of a hydrogen bond.

RESULTS

Wild-Type and R481K CcO Loop and Key Residue Movements. A long loop (residues 152−190), connecting helices III and IV, is on the exterior side near the center of the membrane-spanning region formed by the 12 transmembrane helices of subunit I. This loop has mostly hydrophobic residues (~70%) and makes hydrophobic contacts with helices II, VI, and VII of subunit I. It contains the two highly conserved residues, W172 and Y175 (Figure 2). In the *Rs* crystal structure (*14*), the hydroxyl group of Y175 sits between a water molecule's oxygen atom with a heavy atom distance of 3.16 Å and the ring nitrogen of residue W280 (on helix VI, adjacent to the loop region) with a heavy atom distance of 3.18 Å. The side chain nitrogen of W172 is in hydrogen bonding contact (3.06 Å) with the D-propionate carboxylate oxygen of heme a_3. There are some hydrogen bonds between the loop's few polar residues and other side chains of the nearby helices. During the MD simulation of both the wild type and the R481K mutant, this loop region changes its conformation and shifts some of its amino acids and their hydrogen bonding away from those positions shown in the crystal structure.

After a 1.4 ns simulation, the rmsd of the wild-type C*c*O structure when overlaid, using the main chain atoms, with

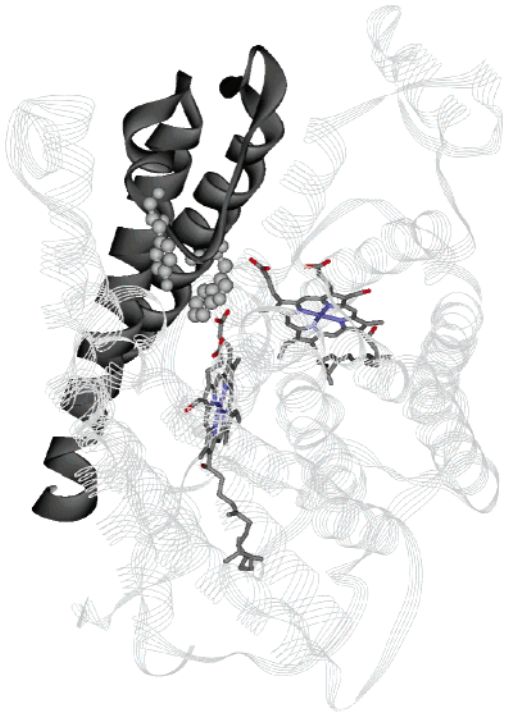

FIGURE 2: Helices III and IV and the loop (residues 152−190) between them, with residues W172 and Y175 displayed as ball-and-stick figures, from the *Rs* crystal structure (*14*).

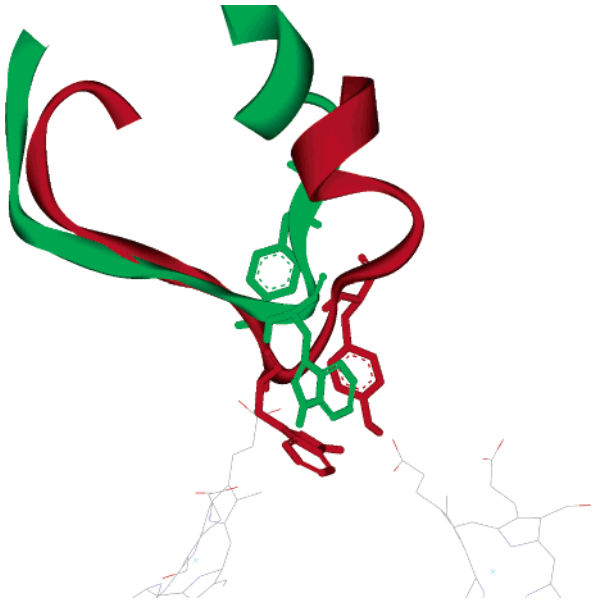

FIGURE 3: Overlay of the wild-type (green) and R481K mutant (red) loops of residues 152−190. Residues W172 and Y175 of the wild type and R481K mutant are shown in their respective colors.

the R481K mutant at the same time frame is 5.2 Å. Comparing the movements of the helix III−helix IV loop (residues 152−190) in the wild type and R481K mutant of this superposed structure shows that the mutant backbone structure containing residues 172−183 drops substantially relative to the wild type (Figure 3). This movement leads to a large drop in residues 176 and 177 of the R481K mutant, along with rearrangements in side chains between the wild-type enzyme and the R481K mutant. The mutant and wild-type overlay shows that the wild-type C_α of W172 is shifted 4.4 Å compared to the same carbon of W172 in the R481K mutant, while the Y175 C_α atom is approximately 6 Å from

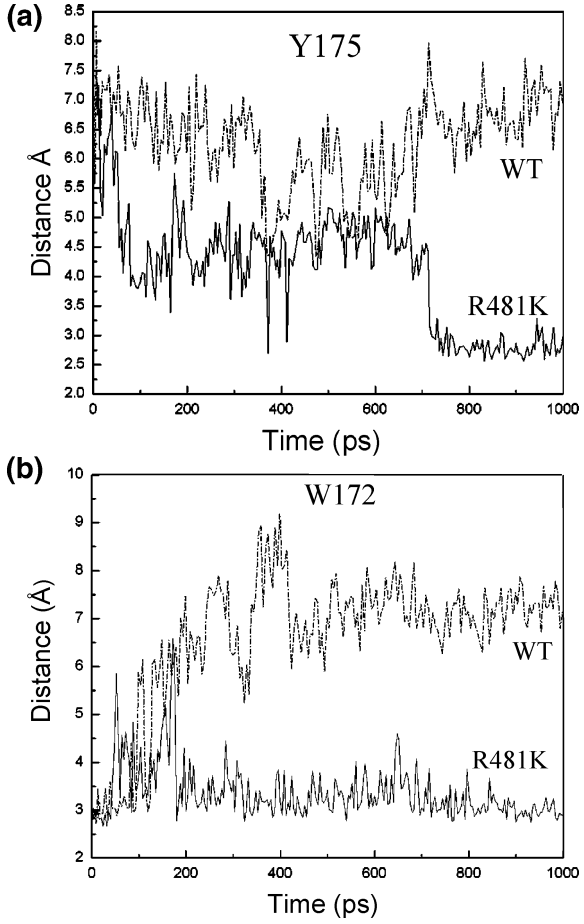

FIGURE 4: (a) Distance (angstroms) between the Y175 hydroxyl oxygen and the carboxyl group of heme a_3 D-propionate for the wild type and R481K mutant over 1 ns of simulation time. (b) Distance (angstroms) between the ring nitrogen of W172 and a heme a_3 D-propionate oxygen. The wild-type W172 increases its distance from the heme a_3 D-propionate to hydrogen bond with E286, while in the mutant, W172 does not move much.

its twin atom in the mutant enzyme. The main chain atoms of residues 172−182 of the loop, on the right side in Figure 3, show larger deviations from those of the wild type than do the residues on the left side.

In the simulation of wild-type C*c*O, the C_α atom of Y175 translates from its crystallographic position by ~4 Å and makes hydrogen bonding contact with the A-propionate carboxylate of heme *a*. In the mutant, by contrast, a structural rearrangement of Y175 moves its hydroxyl within hydrogen bonding distance (2.60 Å) of the heme a_3 D-propionate (Figure 4a). In the WT crystal structure, W172 in the loop between helix III and helix IV of the crystal structure has its ring nitrogen within 3.1 Å of O2D of heme a_3 D-propionate and 7.7 Å from OE2 of E286. W172 and E286 are proposed to be involved in proton translocation events in which E286 passes a proton to W172 (*3*, *15*). Examination of the trajectory data for these two residues reveals that, early in the wild-type MD simulation (~20 ps), the E286 carboxylate rotates to a point that is higher, in the frame of reference in Figure 1, and it maintains this position throughout the simulation (*3*). A similar rotation occurs for the side chain of W172 very early in the simulation, and this orientation is maintained after ~300 ps in the wild-type simulation (Figure 4b). The reorientation of these residues establishes a hydrogen bond between NE1 of W172 (ring) and the O2 (carboxylate) atom of E286 (Figure 5). As with the wild type, the E286 carboxylate in the R481K mutant rotates to point further up within the first few picoseconds. However, unlike the wild type, there is no concomitant movement of W172 to establish hydrogen bonding with E286. Instead, the side chain of W172 initially moves and forms a hydrogen bond with the heme a_3 D-propionate at a distance of ~3.0 Å. Furthermore, in the R481K mutant, the Nϵ atom of W172 is never observed to interact with E286 during the simulation.

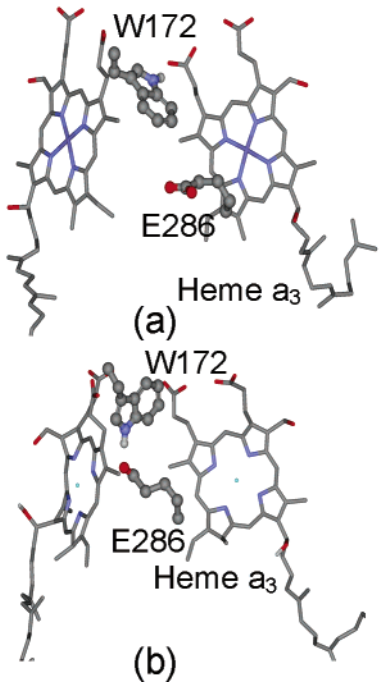

FIGURE 5: Wild-type simulation that leads to hydrogen bond formation between NE1 of W172 and OE2 of E286. (a) The crystal structure shows the hydrogen bonding between the nitrogen on W172 and oxygen on the heme a_3 D-propionate. (b) Early in the simulation (see Figure 4b), the W172 establishes a hydrogen bond with E286.

Heme Interactions and Water Chain Formation of the Wild Type. In the wild-type crystal structure, the heme *a* A-propionate hydrogen bonds to both the backbone nitrogen of R482 and the hydroxyl group of Y414 while the D-propionate hydrogen bonds to both the (NH2) amino group of R481 and Nϵ of R482. These interactions fluctuate some during the simulation but stay characteristically similar. For example, the A-propionate loses its interaction with the R482 backbone in exchange for its interaction with Nϵ of R481. But, in all the MD snapshots that have been examined, the heme *a* A- and D-propionates interact with these arginines. Another conserved arginine (R52) that is known to be important for the spectral and redox potential properties of heme *a* (*40*, *41*) never, in all the MD snapshots that have been examined, strays from its specific hydrogen bonding interaction with the heme *a* formyl group. The crystal structure shows that the D-propionate of heme a_3 is within hydrogen bonding distance (3.0 Å) of NE1 of W172 and in the proximity of the NH1 amino group of R481 (3.21 Å). The A-propionate of heme a_3 hydrogen bonds to ND1 of H411, a ligand of Mg^{2+}, and is within 2.7 Å of the D407 carboxylate group. However, as expected, early in the simulation (~200 ps) D407 moves to a position >9 Å from

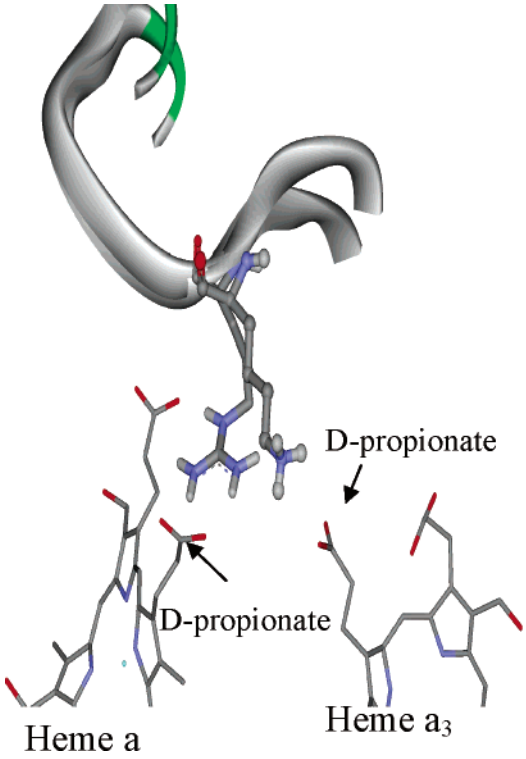

FIGURE 6: Position of residue 481 for the wild type (R481) using stick representation and the mutant (K481) using ball-and-stick representation. The K481 side chain moves from its initial association with the heme *a* D-propionate to form a salt bridge with the heme a_3 D-propionate with a NZ K481−D-propionate carbon distance of ~3.75 Å.

the heme a_3 A-propionate, out toward the bulk water, due to electrostatic repulsion.

During the simulation, water moves into the region above the heme a_3 and supports multiple hydrogen bonding networks. They interact with the heme a_3 propionates, the adjacent R481 and R482 residues, and Mg^{2+}. At times, these waters act as links that connect heme *a*, heme a_3, and R481. The bridging water between the D- and A-propionates of heme a_3 is persistent and appears in all simulation snapshots that have been examined. In addition, the heme a_3 propionate region and above (i.e., the Mg^{2+} area) becomes well-populated with waters, while the complementary region of the A-propionate of heme *a* remains mostly water free, and continues to interact with the amino acid residues, Y414, and R482.

Heme Interactions and Water Chain Formation of the R481K Mutant. As noted above, throughout the MD simulation, W172 does not significantly move in the R481K mutant but remains close to its initial crystal structure position where its NE1 is hydrogen bonded to the heme a_3 D-propionate, and Y175 moves to hydrogen bond its hydroxyl with the D-propionate of heme a_3. After approximately 1 ns, K481 altered its location from that of the wild-type's R481 position and moved closer to the D-propionate of heme a_3 (NZ R481−OE1 D-propionate distance of ~3.3 Å) having formed a salt bridge-like interaction and, concomitantly, increased its distance from the D-propionate of heme *a* to >5 Å, as shown in Figure 6. A water (or waters) in the area between heme *a* and a_3 allows heme *a* to form a water chain to heme a_3, similar to what is found in the wild-type simulation, but now involving Y175. Early in the simulation, there is a loss of hydrogen bonding of R52 to the formyl group of heme *a*, as its NH1 undergoes an increase (to 4.7 Å) in its distance from the formyl group. However, at later times, R52 does return to a distance that allows hydrogen bonding between NH1 of R52 and the heme *a* formyl group.

Water Chain Formation from E286 to Heme a_3 and the Binuclear Center. The region of C*c*O encompassing E286, heme a_3 propionates, and the Fe_{a3}−Cu_B binuclear center has been suggested to be part of a possible chemical and proton pumping pathway (*14*, *21*, *22*). The formation of hydrogen-bonded water chains, emanating from E286 and leading to the D-propionate of heme a_3 and to the binuclear center, can be probed by defining a number of channels (see Computational Methodology) where all of the channels originate on the E286 carboxylate. Since glutamates and propionates are bifunctional (two oxygens) hydrogen bond acceptors, four channels between E286 and the D-propionate are defined, all with a radius of 10 Å. Two more are defined from E286 carboxylate oxygens to the heme a_3 Fe and two more to the Cu_B, also with a radius of 10 Å. Data for all eight channels were collected every 0.1 ps and analyzed for the formation of hydrogen-bonded chains with at least three waters between initial and final atoms in each cylinder. Note that the root (terminator) water has to be hydrogen bonded to the initial (final) atom of the cylinder. The criterion for hydrogen-bonded waters was the severe one (see Computational Methodology) in which $d_{Oa-Ob} < 3.0$ Å and $145° < A_{Oa-H-Ob} < 180°$. The choice of at least three waters in the definition of a chain was made because the cylinders range in length from approximately 12 to 15 Å. The analysis was carried out over a 400 ps interval of data after a simulation time of 1.2 ns.

Connection of E286 to the Heme a_3 D-Propionate and the Binuclear Center. For wild-type C*c*O, the simulation data for the channels between E286 and the heme a_3 D-propionate show that numerous water chains form. The chains are at least six waters long and are present ~2.5% of the time. A typical chain is displayed in Figure 7a. The water chain is conducted to the D-propionate in a "tube" formed by hydrophobic residues V173, L174, P176, and L279 and highly conserved residues W172, W280, F282, and G283. This tube involves the loop of residues 152−190 between helices III and IV and residues 279−282 of helix VI (Figure 7b). The two channels between E286 and Cu_B lead to similar results, since chains that span E286 and the D-propionate also tend to reach Cu_B. For example, the water chain displayed in Figure 7b leads to the binuclear center by the addition of one more water that branches off toward Cu_B. In contrast, the two channels from E286 to the heme a_3 Fe are completely devoid of water chains. There are no waters close to the a_3 Fe to provide a termination point for a chain.

The results for the mutant are completely different from those of the wild type. No water chains were detected within the eight channels that were analyzed. What is quite remarkable is that there are approximately the same numbers of waters (~20) at any instant of time in the channels for the wild type and mutant. Thus, the difference must be related to the arrangement of the waters induced by differences in the wild-type and mutant structures.

Water Chain Formation from E286 to Mg^{2+}. There is also a substantial difference between the wild-type and mutant C*c*O in the region between E286 and Mg^{2+}. A typical wild-

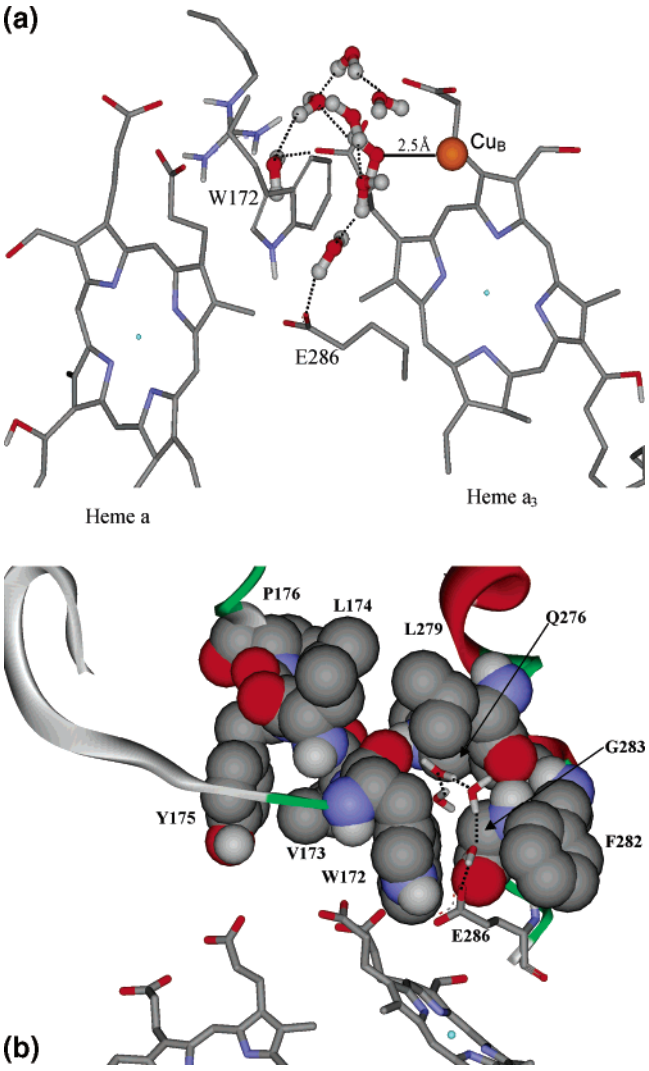

FIGURE 7: (a) Representative hydrogen-bonded water chain in wild-type C*c*O that connects both the carboxylate of E286 with the heme a_3 D-propionate and Cu_B of the binuclear center. (b) Space-filling representation of the hydrogen-bonded water chain in wild-type C*c*O that connects the carboxylate of E286 with the heme a_3 D-propionate (see panel a). The residues that form a tube for water chain formation are indicated in space-filling representation.

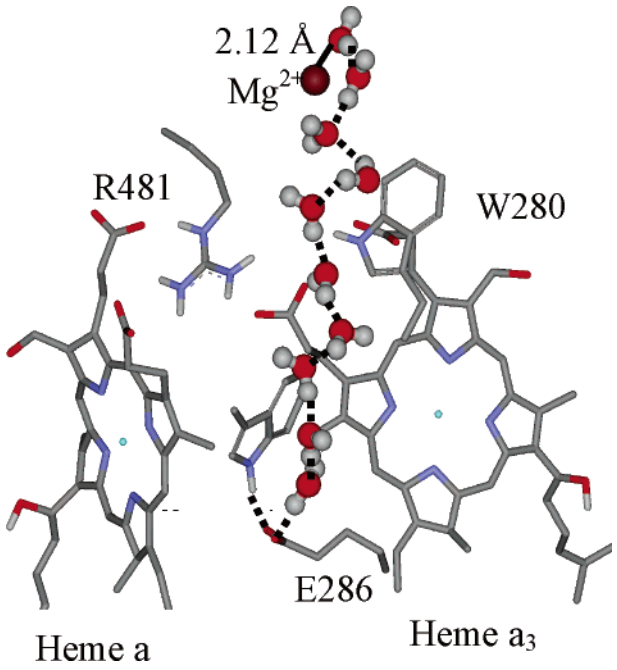

FIGURE 8: Representative hydrogen-bonded water chain in wild-type C*c*O that connects the carboxylate of E286 with Mg^{2+}.

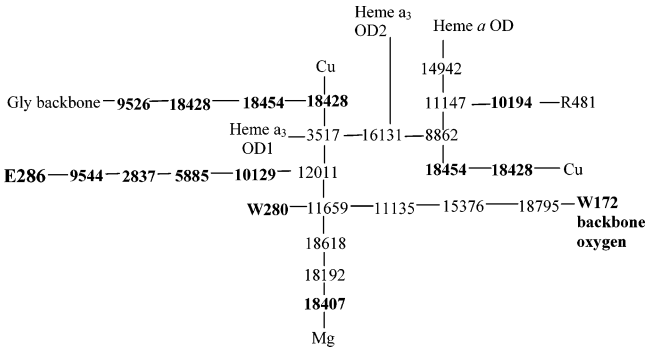

FIGURE 9: Diagram of a hydrogen-bonded network of waters and residues in the region among E286, the binuclear center, and Mg^{2+}. Persistent waters are indicated in boldface type.

Table 1: Hydrogen-Bonded Water Chains Spanning Glu286 to Mg^{2+}

	% time H-bonded in a 200 ps interval	
C*c*O	after 1.4 ns[a]	after 2.4 ns[a]
WT	2.1	26.4
R481K	0.0	5.6

[a] Total time of the simulation.

type water chain spanning E286 to Mg^{2+} is shown in Figure 8 and schematized in Figure 9. The water again is conducted through the hydrophobic tube noted above, but now the chain continues and comes out of the tube leading toward the Mg^{2+}. These latter waters, on the other side of the tube, are also in hydrogen bond contact with polar residues such as W280 and E276 on helix VI, which interact with the water chain leading to Mg^{2+}. For the data collected after 2.4 ns, these wild-type chains consist of 7−16 waters, and have a convoluted structure. The water chains also have side branches, as indicated in Figure 9, and the branching of the water chains tends to increase toward the Mg^{2+} end of the channel. To compare qualitatively water chains in this channel for the wild type and mutant, it is simplest to consider the frequency of chain formation as a function of simulation time. Table 1 lists the percentage of formation of water chains in 200 ps intervals for the wild type and mutant that are present after 1.4 and 2.4 ns of simulation time. That is, after a given simulation time, the number of water chains in a 200 ps interval relative to the 2000 (200 ps/0.1 ps) samples in that interval is obtained. For the 2.4 ns data, the chains in R481K C*c*O are of length between 5 and 12 and, while also branched, provide shorter and more direct connections between E286 and Mg^{2+} than for the wild type. Clearly, water chain formation in R481K is much more difficult than in wild-type C*c*O.

DISCUSSION

Proton translocation in proteins is thought to be promoted through hydrogen-bonded water chains in combination, potentially, with hydrogen bond donor and acceptor residue side chains and peptide carbonyl and imino groups. In C*c*O, one channel, termed the D pathway (*11*) starts at D132 on the cytoplasmic side and continues to E286, which is

approximately 12 Å from the Fe of heme *a* and the Fe of heme a_3. In the *Rs* C*c*O crystal structure, the D132−E286 distance is approximately 30 Å (*14*) (Figure 1), and there are a number of crystallographically defined waters in this D channel. In a recent simulation (*3*), hydrogen-bonded chains of water extending from D132 to N140 and from N140 to E286 were found, but there were no continuous chains spanning E286 and D132. Some of the waters found in this simulation are hydrogen bonded to residues that are also seen to be hydrogen bonded to water in the crystal structure.

Hydrogen-bonded waters that could serve as proton pathways from E286 toward the binuclear center (heme a_3/Cu_B) were not identified in the crystal structures (*14*, *28*, *42*−*44*). This region has been identified as a source of chemical protons for the reduction of oxygen to water (*14*, *45*, *46*). As previously documented (*3*), continuous chains of hydrogen-bonded waters spanning the carboxylate of E286 to Mg^{2+} were observed in the simulation of wild-type C*c*O. A typical chain shown in Figure 8 consists of 10 hydrogen-bonded waters with a water hydrogen-bonded to the carboxylate of E286 and one ligated to Mg^{2+}. These water chains became more numerous the longer the MD simulation was run until saturation set in around 3 ns. For example, after 1.4 (2.4) ns of MD, in the following 200 ps interval, continuous water chains spanning E286 to Mg^{2+} were present for 2.1% (26.5%) of the time. In contrast, for the R481K mutant, no water chains formed in the 200 ps interval after 1.4 ns of simulation and chains were present for only 5.6% of the 200 ps after 2.4 ns of MD (Table 1).

Another significant contrast between the wild type and mutant was found by examining water chain formation starting at the carboxylate of E286 and extending to the D-propionate of heme a_3, and to the Cu_B and Fe of the binuclear center. In the wild type, numerous water chains that span E286 to the heme a_3 D-propionate (Figure 7a) and to Cu_B are formed (Figure 7b). There are multiple shared waters that branch in a complex fashion to the heme a_3 D-propionate and Cu_B sites, and to peptide backbone H-bond acceptors (Figure 9). On the other hand, no chains were found that lead from E286 to the heme a_3 Fe. Of course, there may be waters associated with this Fe; however, they are not part of hydrogen-bonded chains that connect with E286. No water chains from E286 to the A-propionate of heme a_3 were found, but a chain was observed that spanned E286 to the heme *a* D-propionate (Figure 9). The web of waters leading from E286 consists of both persistent waters, defined operationally as waters that move less than 2.0 Å in 100 ps, and transient waters that move more than 2.0 Å during this time interval. Some of the persistent waters are hydrogen bonded to Cu_B, R481, the Gly backbone, and Mg^{2+}. While it is tempting to conclude that persistent waters are associated with charged residues, there are numerous violations of this supposition. Nevertheless, the simulation data do support the conclusion that Mg^{2+} and Cu_B are associated with persistent waters. Persistent waters could be the scaffolding onto which other waters hydrogen bond and form a web of water that stretches from E286 to specific sites to translocate protons. For example, the water chains to the Cu_B of the binuclear active site and Mg^{2+} are ideal candidates for the movement of protons either for pumping (movement of protons to the outside) or for delivering protons to the active site. This is because proton movement to these two sites is expected to be transitory, and should be regulated not to occur at certain stages of the catalytic cycle. In contrast with the wild-type simulation, no water chains connecting E286 with the heme a_3 propionates or to the binuclear center were detected in R481K in the 400 ps examined after 1.4 ns of simulation time. Of course, on the limited MD time scale, we cannot conclude that such water chains do not form in the R481K mutant. But, it is appropriate to assert that they will form more slowly and/or be present for a smaller fraction of the time than in the wild-type enzyme.

Consequently, if water chains spanning E286 to the binuclear center are to serve as proton carriers, one would expect that, in the case of the R481K mutant, proton pumping or oxygen reduction would be slowed to some extent due to a reduction in the extent of water chain formation. That does indeed seem to be the case (*1*). When the R481K mutant is placed in reconstituted vesicles, and exposed to both a membrane potential and a pH gradient, its activity (oxygen reduction) is diminished to a value similar to that of the D132A mutant (accompanying paper by Mills et al. and refs *1* and *47*). In addition, proton pumping is also slowed, although it is still observed (*1*). Furthermore, experimental evidence suggests that the redox potential of heme *a* is lowered in this mutant relative to the wild type, and as a consequence, reduction of heme a_3 occurs more slowly (F.-M. Mills et al., manuscript in preparation). Because of the close coupling of electron and proton movement in C*c*O, it is difficult to delineate whether the electron or proton movement is problematical in such cases. However, a mechanism for this inhibition is suggested by these simulations, which shows a dramatic difference between the wild type and mutant in water chain formation in the region connecting E286 and the binuclear center.

In wild-type C*c*O, part of the water−proton conduit from E286 to heme a_3 D-propionate and Cu_B involves a mainly hydrophobic tube formed by the subunit I residues: W172, V173, L174, P176, L279, W280, F282, and G283. In Figure 7b, a MD snapshot of wild-type C*c*O is shown with a water chain consisting of multiple water molecules extending into the hydrophobic tube. The first five of these waters, 9544, 2837, 5885, 10129, and 1211, diagrammed in Figure 9, extend from E286 through this hydrophobic tube, with the last two waters (outside of the tube) making contact with Cu_B and the heme a_3 D-propionate. These waters act as anchors for creating a complicated web of contacts in this region of the enzyme. For example, the third water (5885 in Figure 9) in the hydrophobic tube hydrogen bonds to the backbone oxygen of W172, and this residue hydrogen bonds to another water molecule, forming a separate water chain that extends to W280. Residues V173, L174, P176, Q276, and W280 form a tubelike structure and surround the latter chain. Interestingly, this chain (consisting of four waters) connects to the former chain's water (12011), which terminates at the Cu_B and heme a_3 D-propionate sites. Leading from water 12011 is another chain that consists of five water molecules connecting the binuclear active site to the Mg^{2+}.

As noted above, in the R481K mutant, water chains extending from E286 to the binuclear center were not observed. The secondary structure of the loop connecting helix III to helix IV and its key residue side chains exhibit substantial rearrangements in the mutant. This large-scale

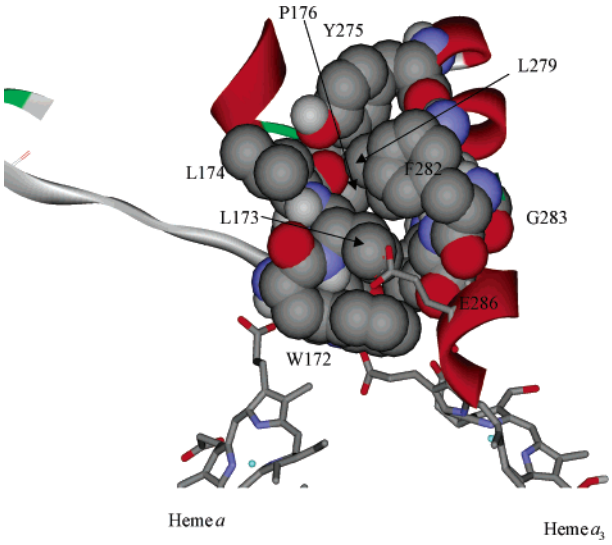

FIGURE 10: Residues of the mutant in space-filling representation that, in the wild type (compare to Figure 7b), form a tube for water chain formation. The movement of the loop of residues 152−190 in the mutant closes the tube that is present in the wild type.

movement results in blockage of what was the hydrophobic water tube in the wild type (Figure 7b), as displayed in Figure 10. In the mutant, W172 maintains an orientation that allows its NE1 atom to hydrogen bond to the heme a_3 D-propionate, instead of to E286, as is the case in the wild-type simulation (*28*, *44*). In the mutant, residues F282, L279, W280, V173, and P176 lining the hydrophobic channel collapse into the water channel and act as barriers to water chain formation. The displacement of V173 and P176 into the channel can be attributed to a drop of the loop's backbone relative to the wild-type structure found around 1.4 ns. The main chain reorientation positions V173 and P176 directly into the hydrophobic tube, which strongly contributes to its closure. These results suggest that the positioning of the loop of residues 152−190 and some special residues in the loop are critical in allowing water chain formation in the region between E286 and the binuclear center.

Our observations that contrast the loop movements of wild-type and mutant C*c*O suggest a possible method for the control of proton/water movement reminiscent of proton pumping proposals for bacteriorhodopsin (*48*). In bacteriorhodopsin, proton pumping is stimulated by a light-induced, water-mediated event, in which the final step of reprotonation of the chromophore involves the formation of a transient water chain that carries a proton from an aspartate residue to the retinal Schiff base in the enzyme interior. This water chain is not present during earlier phases of the reaction cycle due to a constriction of the hydrophobic region, which prevents water access (*48*). In C*c*O, a similar mechanism may be envisioned whereby proton/water migration through the hydrophobic channel between the hemes is inhibited by a narrowing of the channel, during specific parts of the oxidase cycle. In this model, the closing of the hydrophobic channel would be coordinated with, or induced by, movement of W172. That is, when W172 is in hydrogen bonding contact with E286, the hydrophobic channel would be open. This conformation would allow water chain formation and proton translocation. Breakage of hydrogen bonding contact between E286 and W172 by some conformational change could lead to (or be a consequence of) the closing of the hydrophobic channel. In all our wild-type simulation data, when E286 makes hydrogen bonding contact with W172 the hydrophobic channel is open and there is water chain formation. Conversely, if hydrogen bonding contact between these two residues is absent, as in the mutant simulation, the hydrophobic channel is closed.

In the proposed scheme, proton movements from E286 to the binuclear center, to the heme a_3 D-propionate, and to Mg^{2+} are all regulated. In the case of the first two sites, protons are delivered for oxygen chemistry, while for the latter, they could be for proton pumping. Experimental studies have suggested that the propionates could be involved in proton movement in association with R481. The mechanism may involve a modulation of the pK_a of the propionates (most probably the D-propionates of heme *a* and/or a_3) by, for example, altering the proximity of R481 to the heme a_3 D-propionate causing the movement of the W172 away from the propionate group (*47*, *49*, *50*). Certainly, W172 is important in maintaining an active enzyme (*15*).

In C*c*O, protons must maintain a forward movement through the protein to prevent unproductive proton reversal (back leak). The flexibility of the region around the hemes, seen in the MD, suggests a mechanism for collapsing a water channel and preventing protons above the heme from moving back to a deprotonated E286. This could be the "gating" mechanism.

Additionally, although the area above Mg^{2+} is quite hydrated (*3*), it is probable that proton movement to the bulk water is still controlled by the protein to prevent the kinetically significant backward flow of protons and to allow control of proton release. There are several charged amino acids in the exit route of other proton pumps such as bacteriorhodopsin (two glutamates and an arginine) (*48*) and the bc_1 complex (heme b_L propionate, a glutamate, several waters, and an asparagine) (*51*). The particular path for proton exit to the outside in C*c*O has yet to be resolved, but these studies identify certain key residues that may have a role in proton movement, which could be further addressed using experimental and computational methods.

The current MD study, carried out with both hemes in the reduced state, cannot address how the movement of protons might be alternately directed to the active site or for pumping. During the catalytic cycle, various heme reductions and oxidations occur that likely alter conformations because of the tight coupling of electron and proton transfer in C*c*O. Additionally, there is evidence that water formed at the active site during oxygen reduction moves to the Mg^{2+} for release to the outside (*52*). However, the path for protons does not necessarily involve movement through the active site; water and proton exit may follow distinct paths. Simulations can be done with charges designed to represent the various oxidation states during the C*c*O cycle, and they should help address these issues.

REFERENCES

1. Qian, J., Mills, D. A., Geren, L., Wang, K. F., Hoganson, C. W., Schmidt, B., Hiser, C., Babcock, G. T., Durham, B., Millett, F., and Ferguson-Miller, S. (2004) Role of the conserved arginine pair in proton and electron transfer in cytochrome *c* oxidase, *Biochemistry 43*, 5748−5756.
2. Voet, D., and Voet, J. G. (1990) *Biochemistry*, John Wiley & Sons, New York.

3. Cukier, R. I. (2004) Quantum molecular dynamics simulation of proton transfer in cytochrome *c* oxidase, *Biochim. Biophys. Acta 1656*, 189−202.
4. Cukier, R. I. (2004) Theory and simulation of proton-coupled electron transfer, hydrogen-atom transfer, and proton translocation in proteins, *Biochim. Biophys. Acta 1655*, 37−44.
5. Mills, D. A., and Ferguson-Miller, S. (2003) Understanding the mechanism of proton movement linked to oxygen reduction in cytochrome *c* oxidase: Lessons from other proteins, *FEBS Lett. 545*, 47−51.
6. Zaslavsky, D., and Gennis, R. B. (2000) Proton pumping by cytochrome oxidase: Progress, problems and postulates, *Biochim. Biophys. Acta 1458*, 164−179.
7. Mitchell, R., and Rich, P. R. (1994) Proton Uptake by Cytochrome-C-Oxidase on Reduction and on Ligand-Binding, *Biochim. Biophys. Acta 1186*, 19−26.
8. Artzatbanov, V. Y., Konstantinov, A., and Skulachev, V. (1978) Involvement of intramitochondrial protons in redox reactions of cytochrome a, *FEBS Lett. 87*, 180−185.
9. Capitanio, N., Capitanio, G., Minuto, M., De Nitto, E., Palese, L. L., Nicholls, P., and Papa, S. (2000) Coupling of electron transfer with proton transfer at heme a and Cu(A) (redox Bohr effects) in cytochrome *c* oxidase. Studies with the carbon monoxide inhibited enzyme, *Biochemistry 39*, 6373−6379.
10. Michel, H. (1999) Cytochrome *c* Oxidase: Catalytic Cycle and Mechanisms of Proton Pumping-A Discussion, *Biochemistry 38*, 15129−15140.
11. Konstantinov, A. A., Siletsky, S., Mitchell, D., Kaulen, A., and Gennis, R. (1997) The Roles of the Two Proton Input Channels in Cytochrome *c* Oxidase from *Rhodobacter sphaeroides* Probed by the Effects of Site-directed Mutations on Time-resolved Electrogenic Intraprotein Proton Transfer, *Proc. Natl. Acad. Sci. U.S.A. 94*, 9085−9090.
12. Branden, M., Sigurdson, H., Namslauer, A., Gennis, R., Adelroth, P., and Brzezinski, P. (2001) On the role of the K-proton-transfer pathway in cytochrome *c* oxidase, *Proc. Natl. Acad. Sci. U.S.A. 98*, 5013−5018.
13. Adelroth, P., Ek, M. S., Mitchell, D. M., Gennis, R. B., and Brzezinski, P. (1997) Glutamate 286 in cytochrome aa3 from *Rhodobacter sphaeroides* is involved in proton uptake during the reaction of the fully-reduced enzyme with dioxygen, *Biochemistry 36*, 13824−13829.
14. Svensson-Ek, M., Abramson, J., Larsson, G., Tornoth, S., Brzezinski, P., and Iwata, S. (2002) The X-ray crystal structures of wild-type and EQ(I-286) mutant cytochrome *c* oxidases from *Rhodobacter sphaeroides*, *J. Mol. Biol. 321*, 329−339.
15. Behr, J., Michel, H., Mäntele, W., and Hellwig, P. (2000) Functional Properties of the Heme Propionates in Cytochrome *c* Oxidase from *Paracoccus denitrificans*. Evidence from FTIR Difference Spectroscopy and Site-Directed Mutagenesis, *Biochemistry 39*, 1356−1363.
16. Puustinen, A., and Wikstrom, M. (1999) Proton exit from the heme-copper oxidase of *Escherichia coli*, *Proc. Natl. Acad. Sci. U.S.A. 96*, 35−37.
17. Nagle, J. F., and Tristam-Nagle, S. (1983) Hydrogen Bonded Chain Mechanisms for Proton Conduction and Proton Pumping, *J. Membr. Biol. 74*, 1−14.
18. Agmon, N. (1995) The Grotthuss Mechanism, *Chem. Phys. Lett. 244*, 456−462.
19. Iwata, S., Ostermeier, C., Ludwig, B., and Michel, H. (1995) Structure at 2.8 Å resolution of cytochrome *c* oxidase from *Paracoccus denitrificans*, *Nature 376*, 660−669.
20. Pomes, R., and Roux, B. (1998) Free energy profiles for H^+ conduction along hydrogen-bonded chains of water molecules, *Biophys. J. 75*, 33−40.
21. Stuchebrukhov, A. A. (2003) Electron-transfer reactions coupled to proton translocation. Cytochrome oxidase, proton pumps, and biological energy transduction, *J. Theor. Comput. Chem. 2*, 91−118.
22. Wikstrom, M., Verkhovsky, M. I., and Hummer, G. (2003) Water-gated mechanism of proton translocation by cytochrome *c* oxidase, *Biochim. Biophys. Acta 1604*, 61−65.
23. Pomes, R., Hummer, G., and Wikstrom, M. (1998) Structure and dynamics of a proton shuttle in cytochrome *c* oxidase, *Biochim. Biophys. Acta 1365*, 255−260.
24. Zheng, X., Medvedev, D. M., Swanson, J., and Stuchebrukhov, A. A. (2003) Computer simulation of water in cytochrome *c* oxidase, *Biochim. Biophys. Acta 1557*, 99−107.
25. Behr, J., Hellwig, P., Mantele, W., and Michel, H. (1998) Redox dependent changes at the heme propionates in cytochrome *c* oxidase from *Paracoccus denitrificans*: Direct evidence from FTIR difference spectroscopy in combination with heme propionate ^{13}C labeling, *Biochemistry 37*, 7400−7406.
26. Behr, J., Michel, H., Mantele, W., and Hellwig, P. (2000) Functional properties of the heme propionates in cytochrome *c* oxidase from *Paracoccus denitrificans*. Evidence from FTIR difference spectroscopy and site-directed mutagenesis, *Biochemistry 39*, 1356−1363.
27. Yoshikawa, S. (2003) A cytochrome *c* oxidase proton pumping mechanism that excludes the O2 reduction site, *FEBS Lett. 555*, 8−12.
28. Ostermeier, C., Harrenga, A., Ermler, U., and Michel, H. (1997) Structure at 2.7 Å resolution of the *Paracoccus denitrificans* two-subunit cytochrome *c* oxidase complexed with an antibody Fv fragment, *Proc. Natl. Acad. Sci. U.S.A. 94*, 10547−10553.
29. Cukier, R. I., and Seibold, S. A. (2002) Molecular Dynamics Simulations of Prostaglandin Endoperoxide II Synthase-1: Role of Water and the Mechanism of Compound I Formation from Hydrogen Peroxide, *J. Phys. Chem. B 106*, 12031−12044.
30. van Gunsteren, W. F., and Berendsen, H. J. C. (1987) *GROMOS Manual*, University of Groningen: Groningen.
31. Hockney, R. W., and Eastwood, J. W. (1981) *Computer simulation using particles*, McGraw-Hill, New York.
32. Allen, M. P., and Tildesley, D. J. (1987) *Computer Simulation of Liquids*, Clarendon Press, Oxford, U.K.
33. Ryckaert, J. P., Ciccotti, G., and Berendsen, H. J. C. (1977) Numerical-Integration of Cartesian Equations of Motion of a System with Constraints: Molecular-Dynamics of *N*-Alkanes, *J. Comput. Phys. 23*, 327−341.
34. Berendsen, H. H. C., Postma, J. P. M., Gunsteren, W. F., DiNola, A., and Haak, J. R. (1984) Molecular dynamics with coupling to an external bath, *J. Chem. Phys. 81*, 3684−3690.
35. Ferguson-Miller, S. (2003) Coordinates.
36. *MOE* (2003) Chemical Computing Co., Montreal, PQ.
37. MacKerell, A. D., Brooks, B. R., Brooks, C. L., III, Nilsson, L., Rous, B., Won, Y., and Karplus, M. (1998) *The Encyclopedia of Computational Chemistry*, Vol. 1, p 271, John Wiley & Sons, Chichester, U.K.
38. Hofacker, I., and Schulten, K. (1998) Oxygen and proton pathways in cytochrome *c* oxidase, *Proteins 30*, 100−107.
39. Solomon, E. I., Sundaram, U. M., and Machonkin, T. E. (1996) Multicopper Oxidases and Oxygenases, *Chem. Rev. 96*, 2563−2605.
40. Jasaitis, A., Backgren, C., Morgan, J., Puustinen, A., Verkhovsky, M. I., and Wikstrom, M. (2001) Electron and proton transfer in the arginine-54-wethionine mutant of cytochrome *c* oxidase from *Paracoccus denitrificans*, *Biochemistry 40*, 5269−5274.
41. Riistama, S., Verkhovsky, M. I., Laakkonen, L., Wikstrom, M., and Puustinen, A. (2000) Interaction between the formyl group of heme a and arginine 54 in cytochrome aa_3 from *Paracoccus denitrificans*, *Biochim. Biophys. Acta 1456*, 1−4.
42. Tsukihara, T., Shimokata, K., Katayama, Y., Shimada, H., Muramoto, K., Aoyoma, H., Mochizuki, M., Shinzawa-Itoh, K., Yamashita, E., Yao, M., Ishimura, Y., and Yoshikawa, S. (2003) The low-spin heme of cytochrome *c* oxidase as the driving element of the proton-pumping process, *Proc. Natl. Acad. Sci. U.S.A. 100*, 15304−15309.
43. Iwata, S., Lee, J. W., Okada, K., Lee, J. K., Iwata, M., Rasmussen, B., Link, T. A., Ramaswamy, S., and Jap, B. K. (1998) Complete structure of the 11-subunit bovine mitochondrial cytochrome bc_1 complex, *Science 281*, 64−71.
44. Tsukihara, T., Aoyama, H., Yamashita, E., Tomizaki, T., Yamaguchi, H., Shinzawa-Itoh, K., Nakashima, R., Yaono, R., and Yoshikawa, S. (1996) The whole structure of the 13-subunit oxidized cytochrome *c* oxidase at 2.8 Å, *Science 272*, 1136−1144.
45. Alderoth, P., Mitchell, D. M., Gennis, R. B., and Brzezinski, P. (1997) Glutamate 286 in Cytochrome aa_3 from *Rhodobacter sphaeroides* is Involved in Proton Uptake During the Reaction of the Fully-Reduced Enzyme with Dioxygen, *Biochemistry 36*, 13824−13829.
46. Adelroth, P., Karpefors, M., Gilderson, G., Tomson, F. L., Gennis, R., and Brzezinski, P. (2000) Proton transfer from glutamate 286 determines the transition rates between oxygen intermediates in cytochrome *c* oxidase, *Biochim. Biophys. Acta 1459*, 533−539.
47. Mills, D. A., and Ferguson-Miller, S. (2002) Influence of structure, pH and membrane potential on proton movement in cytochrome *c* oxidase, *Biochim. Biophys. Acta 1555*, 96−100.

48. Lanyi, J. K., and Luecke, H. (2001) Bacteriorhodopsin, *Curr. Opin. Struct. Biol. 11*, 415−419.
49. Hellwig, P., Rost, B., Kaiser, U., Ostermeier, C., Michel, H., and Mantele, W. (1996) Carboxyl group protonation upon reduction of the *Paracoccus denitrificans* cytochrome *c* oxidase: Direct evidence by FTIR, *FEBS Lett. 385*, 53−57.
50. Hellwig, P., Gryzbek, S., Behr, J., Ludwig, B., Michel, H., and Mantele, W. (1999) Electrochemical and ultraviolet/visible/infrared spectroscopic analysis of heme a and a3 redox reactions in the cytochrome *c* oxidase from *Paracoccus denitrificans*: Separation of heme a and a3 contributions and assignment of vibrational modes, *Biochemistry 38*, 1685−1694.
51. Izrailev, S., Crofts, A. R., Berry, E. A., and Schulten, K. (1999) Steered Molecular Dynamics Simulation of the Rieske Subunit Motion in the Cytochrome bc_1 Complex, *Biophys. J. 77*, 1753−1768.
52. Florens, L., Schmidt, B., McCracken, J., and Ferguson-Miller, S. (2001) Fast deuterium access to the buried magnesium/manganese site in cytochrome *c* oxidase, *Biochemistry 40*, 7491−7497.

BI0502902